Comparison of renewable integration schemes for AC railway power supply system

Kano, Nakaret; Tian, Zhongbei; Chinomi, Nutthaka; Hillmansen, Stuart

DOI:
10.1049/els2.12048

Document Version
Publisher's PDF, also known as Version of record

Citation for published version (Harvard):
Kano, N, Tian, Z, Chinomi, N & Hillmansen, S 2022, 'Comparison of renewable integration schemes for AC railway power supply system', *IET Electrical Systems in Transportation*, vol. 12, no. 3, pp. 209-222. https://doi.org/10.1049/els2.12048

Received: 7 October 2021 | Revised: 9 June 2022 | Accepted: 2 August 2022

IET Electrical Systems in Transportation

DOI: 10.1049/els2.12048

The Institution of Engineering and Technology WILEY

ORIGINAL RESEARCH

Comparison of renewable integration schemes for AC railway power supply system

Nakaret Kano[1] | Zhongbei Tian[2] | Nutthaka Chinomi[2] | Stuart Hillmansen[1]

[1]Electronic, Electrical and Systems Engineering, University of Birmingham, Birmingham, UK

[2]Electrical Engineering and Electronics, University of Liverpool, Liverpool, UK

Correspondence

Zhongbei Tian, Department of Electrical Engineering and Electronics, University of Liverpool, Liverpool L69 3GJ, UK.
Email: Zhongbei.tian@liverpool.ac.uk

Funding information

Decarbonising Transport through Electrification (DTE) Network+ funded by EPSRC, Grant/Award Number: EP/S032053/1

Abstract

To achieve the UK net-zero emissions target by 2050, transformations to decarbonise the energy system will be essential. A transition from generating electricity by burning fossil fuel to renewable energy sources (RESs) is one of the most effective ways, in addition to customer transformation, in which people are willing to participate to reduce energy consumption. The railway sector accounts for 0.5% of carbon emissions in the United Kingdom. In order to meet the net-zero goal, more railway routes must be electrified, as only 38% of railway routes are electrified at present. Furthermore, clean energy is necessary. Therefore, schemes for integrating RESs into the AC high-speed railway power supply system are proposed and simulated in a case study. Power losses in the power system are comprehensively studied and compared. Owing to the fluctuation of traction load, the power quality issue is inevitable. Thus, the voltage unbalance factor is adopted to measure the severity of the imbalance. The results from the case study demonstrate that the proposed scheme in which the RES is connected to a three-phase railway power network generates the smallest power losses among all proposed schemes. Moreover, it also requires lower investment expenditure and provides the most significant cost saving in the long run. The results also reveal that the VUFs of all schemes based on a 400 kV transmission system are below the United Kingdom's stringent limit of 1.5%. Furthermore, the CO_2 emissions are reduced significantly with RES integration by half for the case study with the 120 MW RES. Although the other proposed schemes had higher losses and lifetime costs, the differences are not significant. Each scheme has its advantages and disadvantages. Several factors need to be considered to choose the suitable scheme, such as the size of land available etc.

KEYWORDS

carbon emission, high-speed train, power losses, power system, railway power system, renewable energy, solar energy, traction power supplies, voltage unbalance factor, wind energy

1 | INTRODUCTION

With the concern about climate change, renewable energy sources (RESs) play a vital role in the field of electricity production, being clean and sustainable. Several countries have set policies to support the use of renewable energy, especially in Europe and the USA. In 2019, the UK government set an ambitious goal to reach net-zero emissions by 2050 [1]. Many sectors, especially the energy supply sector, have started planning to reduce CO_2 emissions. The UK installed capacity of RESs has risen continuously since 2000. According to Ref. [2], the cost of adding new onshore wind farms and solar PV farms is lower than that of other types of new generation units. It was reported that the share of electricity produced from solar power and wind went up from 23.6% in 2019 to 28.3% in 2020, with 88.5 TWh generated [3]. The estimate from the United Kingdom's Department for Business, Energy and Industrial Strategy shows a 10.7% reduction in CO_2 emissions in 2020 [3]. The largest contributor to CO_2 emissions is the transport sector, with 27%, followed by the energy supply

sector, which accounts for 21%. Road transport is the main source of emissions, with a share of over 90%. In contrast, railway transport only accounts for 1.4% of the transport sector or 0.5% of the United Kingdom's total emissions [4]. Although electrified trains emit nearly zero emissions at the point of use, the CO_2 emissions come from the power generation process. Integration of RESs into the railway power network may alleviate various issues, especially carbon emissions and the reliance on energy from the national grid. Nevertheless, there are only a few projects implemented in the real world.

There is some interesting research regarding RES integration for railway traction power supply. D'Arco et al. [5] proposed PV integration schemes for AC railways and compared them in terms of cost and power losses. The train energy demand and the solar irradiance in Italy were used in a case study. The study revealed that the PV farm power rating is the critical factor determining the system's cost. Nonetheless, wind farms were not included in the study. A multi-period AC railway optimal power flow problem formulated by considering PV plants and wind turbines was introduced by Aguado et al. [6]. The authors also included the utilisation of a hybrid energy storage system (HESS) to capture excess energy from the RES and train regenerative braking energy. To analyse the uncertainties of the energy from the RES, a scenario tree approach was employed in the case study, resulting in cost and energy savings of 33.22% and 9.63%, respectively. A Railway Station Energy Management (RSEM) system was proposed by Şengör et al. [7]. The main goal of the RSEM was to effectively reuse the regenerative braking energy from electric trains by using an ESS. Additionally, the PV generator was integrated into the railway power supply system. Mixed-integer linear programing was formulated to solve the optimisation problem. The case study showed that a cost reduction of about 35% was observed when the PV, ESS, and regenerative braking energy were utilised. The abovementioned studies are based on RES integration into the conventional traction substation.

A few scholars presented other approaches for integrating the RESs into a new type of traction substation. Liu et al. [8] proposed a co-phase traction substation (CTSS) energy management system to minimise operating costs, considering the power flow controller and the PV generator and HESS. The study also considered the three-phase unbalance constraint. A two-stage robust optimisation problem was modelled to deal with the PV and train load uncertainties. The goals of the first stage were to find the operating point of the HESS and energy transactions with the grid. The CTSS optimal power dispatch was determined in the second stage. Compared to the conventional traction substation, a cost saving of 4.99% was attained through the proposed methodology. Besides that, the voltage unbalance was well controlled below the maximum admissible constraint of 2% in China. A flexible traction power supply system (FTPSS) was proposed by Chen et al. [9]. A back-to-back converter, HESS, and solar PV plant were integrated into the scheme. Moreover, the authors also presented flexible railway energy management for multiscale optimal dispatch to compensate for the demand and supply imbalance. It was shown in the case study that PV and HESS integration helped reduce the total operational cost of FTPSS by 32.7%.

The existing work has mainly focussed on cost-saving and energy reduction, but details regarding power losses in each component are still not clear. Therefore, this paper presents three schemes for integrating RESs into the railway power network and considers the lifetime cost and power losses of each component relating to RESs. Simulink, based on the MATLAB environment, is used to model and simulate the energy flow for each proposed scheme. The contributions of this paper are as follows:

1) Renewable integration schemes for the 25 kV AC railway power system are proposed. Various sizes of PV farms and wind farms are simulated.
2) The electrical losses, that is, transformer losses, transmission line losses, and inverter losses (including losses in the static converter) of each scheme, are compared comprehensively.
3) The effect of RES integration on the grid is explored, and the voltage unbalance factor (VUF) is calculated for each proposed scheme.
4) The lifetime cost of each proposed scheme with various RES installed capacities is also compared.

This paper is organised as follows: Section 2 introduces the description of the proposed schemes. Section 3 demonstrates the details of each component in the system and the steps for implementation. The case study and results are illustrated in Section 4, followed by the conclusion and future work in Section 5.

2 | SYSTEM DESCRIPTION

The 2 × 25 kV, 50 Hz AC railway power supply system was designed to support the need for the high traction power of high-speed trains. With the issue of poor power quality due to power unbalance, for example, negative-phase current and harmonic distortion, the railway power supply system needs to be connected to a high-voltage power supply point that possesses a high short-circuit capacity.

In this paper, the three-phase 400 kV power system from the national grid is used as the main power supply. The Grid Supply Point (GSP), a substation owned by the national grid, steps down the transmission line voltage to 132 kV before entering the railway traction substation, where traction transformers are located [10]. It is assumed that the electrical power system after the GSP is owned by the railway system operator, seen as the dashed line in Figure 1a, which indicates a responsibility boundary between the national grid and the railway system operator.

A V/V transformer connection is employed to convert three-phase 132 kV power to two single-phase 25 kV (2 × 25 kV) at the traction substation in this study.

A solar PV farm and a wind farm are integrated into the existing power supply system, with different proposed schemes

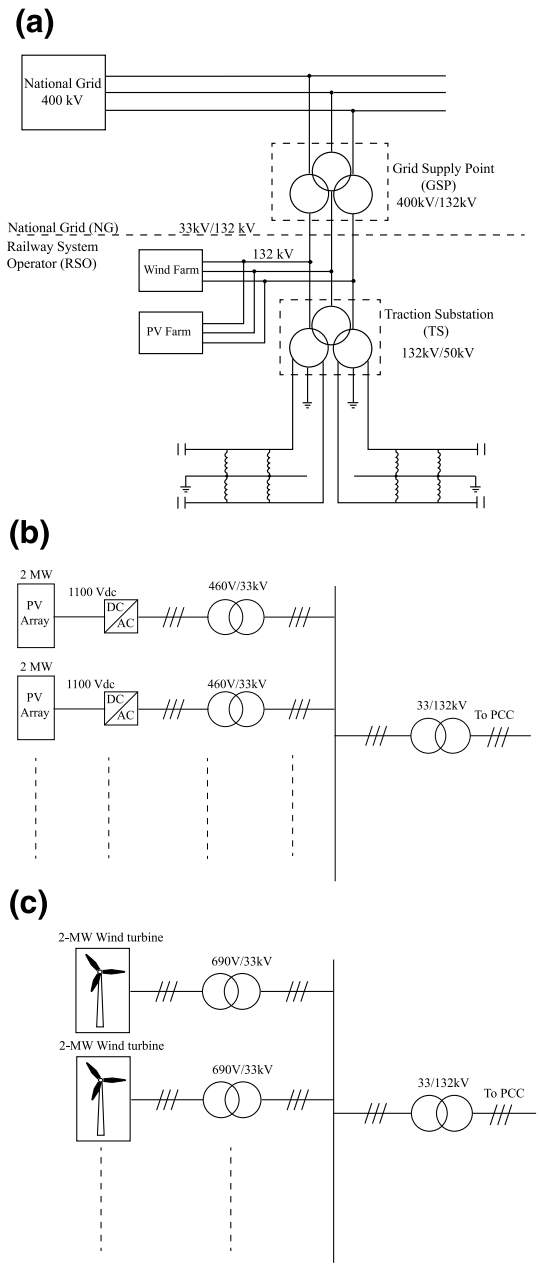

FIGURE 1 (a) Scheme of renewable energy sources connected to the three-phase railway power network, (b) single-line diagram of a solar PV farm, and (c) single-line diagram of a connected wind farm (PCC is a point of common coupling). (b) and (c) are used for scheme-1 and scheme-2

to reduce dependence on power from the national grid, which is mainly generated from fossil fuels. Three renewable energy integration schemes are proposed in this study.

2.1 | RES connected to the three-phase railway power network (Scheme-1)

For this scheme, a three-phase solar PV farm and wind farm are installed and connected to a three-phase 132 kV distribution line at the point between the GSP and the traction substation, as seen in Figure 1a. The PV farm and wind farm locations are assumed to be close enough to share the transmission line and are in the proximity of three-phase railway distribution lines. Therefore, the transmission losses due to the connection of RESs are ignored in this study.

Figure 1b shows a single-line diagram of a solar PV farm implemented in this configuration. The electricity produced from each PV module is a low-voltage direct current. To obtain the required voltage level and power, the PV modules are connected in series and parallel, an arrangement called a PV array. The PV arrays are assumed to always operate at their maximum power point. Generally, for large-scale PV farms, several PV arrays are used to generate the required power, and central inverter topology is used to convert DC power to AC for each array. In this study, the PV farm comprises several sets of PV arrays, each with a 2 MW power capacity. The 1100 V DC output from each PV array is inverted to three-phase 460 V AC power via 2.2 MVA inverters [11]. Then, 2.5 MVA transformers are operated to step up the voltage from 460 kVAC to 33 kVAC. The output of all PV arrays is then combined and raised to 132 kV by a 33 kV/132 kV power transformer to connect to the distribution network.

Similarly, the wind farm is made up of several 2 MW wind turbines. The asynchronous generator with a wound rotor in the turbine generates a three-phase voltage of 690 VAC. For each wind turbine, the voltage is stepped up to 33 kV by a 2.1 MVA transformer located inside the nacelle of the wind turbine [12]. The electricity from each wind turbine then gathers at the collection system and is raised again to 132 kV to connect to the grid system, as seen in Figure 1c.

2.2 | RES connected to railway power supply system via V/V transformer (Scheme-2)

In this scheme, the details of the PV and wind farms are identical to those of the first scheme, excluding the connection point and methods. Both RESs are connected to the V/V transformer (V/V TF), as shown in Figure 2. The primary purpose of this transformer is to convert the three-phase power from both PV and wind farms to a pair of single-phase 25 kV power lines. These 25 kV lines are integrated into the railway at the secondary side of the traction transformer. The PV and wind farms are identical to those of the previous scheme, as seen in Figure 1b,c.

2.3 | RES connected to railway power supply system via static converter (Scheme-3)

This scheme is different from the first two schemes. A smaller RES is connected to the low-voltage side of the traction transformer via a Static Frequency Converter (SFC), as shown in Figure 3a.

The capacity of each PV and wind farm is half that of the first two schemes. However, another set of both is installed and connected at the opposite feeding section. Additionally, it is assumed that there are no transmission losses (PV and wind

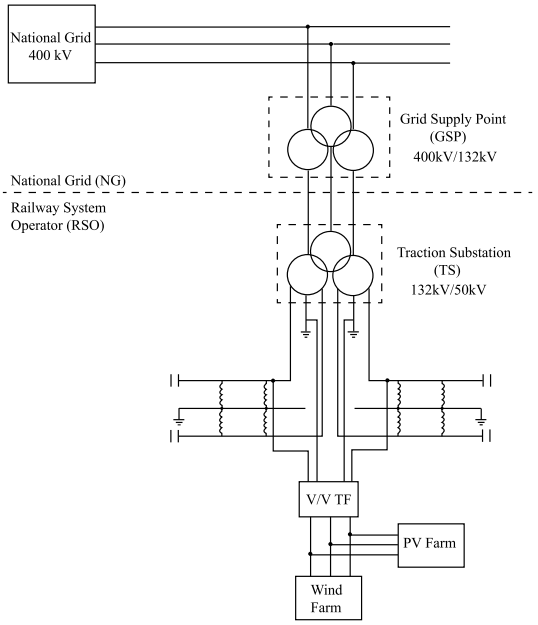

FIGURE 2 Scheme of renewable energy sources connected to the railway power supply system via a V/V transformer

farms are installed near the traction substations). It should be noted that, usually, a megawatt-scale PV farm is transmitted as a three-phase power system. Thus, a special converter, such as a static converter, is required to convert a three-phase 33 kV power system to a single-phase 25 kV power system.

The single-line diagram of the distributed solar PV farm and wind farm is illustrated in Figure 3b. For instance, a 10 MW PV farm consists of five 2 MW PV arrays. The 10 MW wind farm consists of five 2 MW wind turbines. Instead of using power transformers to step up the three-phase voltage of the PV farm and wind farm from 33 to 132 kV in the first two schemes, the SFC is utilised to convert three-phase 33 kV to single-phase 25 kV.

SFCs are widely used in many European countries, for example, Germany, Switzerland and Austria, to convert the frequency from 50/60–16.7 Hz for railway power supply systems [13]. However, according to Ref. [14], an SFC can operate as a three-phase to single-phase converter without converting frequency. For instance, on the Doncaster East Coast Main Line in the United Kingdom, ABB's SFC will be used to convert three-phase 33 kV, 50 Hz to single-phase 25 kV, 50 Hz to feed the traction load [15, 16].

3 | METHODOLOGY

3.1 | Train energy consumption

To calculate train energy demand, the rolling stock specification (train power, maximum traction, and physical properties) and route information (speed limit and gradient) are needed. The movement of the train follows the motion law of Newton as shown in Equation (1) [17]. The train movement

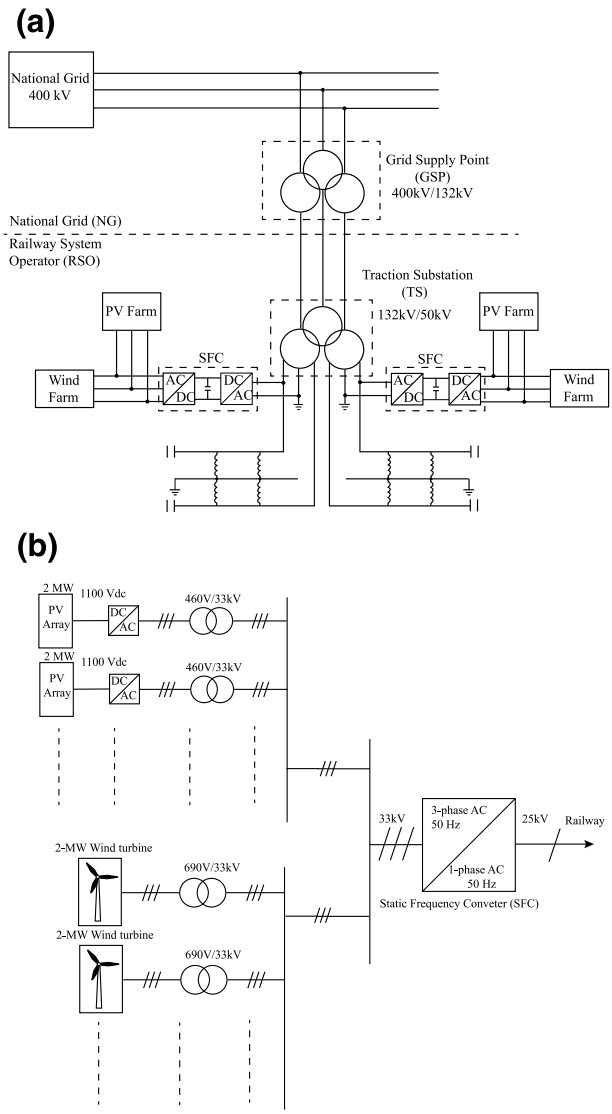

FIGURE 3 (a) Scheme of renewable energy source connected to the railway power supply system via a Static Frequency Converter (SFC), (b) single-line diagram of the solar PV farm and wind farm connected to the railway overhead line via SFC

is impeded by the gradient resistance, Davis resistance, and curve resistance.

$$M_e \cdot a = F - M \cdot g \cdot \sin(\alpha) - F_D - F_C \quad (1)$$

where M_e is the effective mass of the train (kg), a is the train acceleration (m/s^2), F is the tractive force (N), M is the train mass (kg), g is the gravitational acceleration constant (m/s^2), α is the route slope angle (rad), F_D is the resistance due to train motion known as Davis resistance (N), and F_C is the curve resistance (N).

The traction substations not only supply the exact amount of energy that the train requires but also suffer losses on the overhead wire (contact wire) during the current flows to the train. This contact wire loss is modelled and combined with train demand to obtain the total demand; Equation (2) is used to calculate the ohmic line loss in the contact wire.

$$P_{\mathrm{CWloss}} = |I_{\mathrm{CW}}|^2 \cdot R_{\mathrm{cw}} \tag{2}$$

where I_{cw} is the contact line current (A), R_{cw} is the contact wire resistance (Ω), and P_{CWloss} is the contact wire ohmic loss (W).

For electric trains equipped with a regenerative brake, electric power is generated during train braking. If there is a train in traction mode in the same feeding section without interruption of the neutral zone, this regenerative energy will be consumed by that train. Otherwise, it will flow back to the national grid in the case of an AC railway power system.

3.2 | Renewable energy sources

With a decline in cost for installation and operation, the RES installed capacity, especially for solar PV farms and wind farms, keeps increasing.

3.2.1 | Solar PV Farm

The natural light from the sun is the most abundant source of energy. In this paper, the megawatt-scale PV farms are connected to the system in different ways according to the proposed schemes.

A PV model is created in Simulink with a controlled-current source block. Due to the nature of the simulation type (steady-state model), the effect of temperature is ignored. Therefore, solar irradiance is the only input of the PV model. The amount of electrical power from the PV farm is calculated as given in Equation (3) [18]:

$$P_{pv}(s) = s \cdot A \tag{3}$$

The electrical energy generated is computed by

$$E_{pv} = \int_0^t P_{pv} dt \tag{4}$$

where P_{pv} (s) is the power (W) produced by the PV farm, E_{pv} is the energy of the PV farm (Wh), s is the solar irradiance (W/m^2), A is the surface area of the PV farm (m^2), and t is time (s).

The capacity of the PV farm is determined by the PV surface area multiplied by solar irradiance at standard test conditions (1000 W/m^2). For example, a PV farm with a surface area of 1000 m^2 can output up to 1 MW of power.

3.2.2 | Wind Farm

According to Ref. [19], energy generated from wind in 2019 accounted for nearly one-fifth of the UK's total supply and became the second biggest energy source, only behind gas combined-cycle generation.

The electrical power output of a wind turbine is dependent mainly upon wind speed. The turbine will start generating power when the wind speed is higher than the cut-in speed. When the wind speed reaches the cut-out speed, the turbine will shut down to prevent structural damage. To calculate the wind speed at a specific hub height, the reference height of 10 m is used, at which most data sources of the wind speed profile are recorded. The relationship between height and wind speed is shown in Equation (5) [20].

$$v_h = v_0 \cdot \left(\frac{h}{h_0}\right)^{\alpha} \tag{5}$$

where v_h is the wind speed (m/s) at height h, v_0 is the average wind speed (m/s) at height h_0, h is the hub height of the wind turbine (m), h_0 is the referenced height (10 m), and α is the Hellman height exponent.

The value of the Hellman height exponent is assumed to be 0.159, which is used in a location with a small number of wind obstacles [21]. The electrical power produced by a wind turbine is given in Ref. [22] as follows:

$$P_w(v) = \begin{cases} 0, & v < v_{ci} \\ P_r \cdot \dfrac{v^a - v_{ci}^a}{v_r^a - v_{ci}^a}, & v_{ci} \le v \le v_r \\ P_r, & v_r < v < v_{co} \\ 0, & v > v_{co} \end{cases} \tag{6}$$

Energy from the wind turbine is calculated by

$$E_w = \int_0^t P_w dt \tag{7}$$

where P_w is the power output (W) of the turbine, E_w is the energy (Wh) from a wind farm, P_r is the rated power or turbine capacity (W), V is the wind speed (m/s), V_{ci} is the cut-in wind speed (m/s), V_{co} is the cut-out wind speed (m/s), V_r is the rated wind speed (m/s), and a is the Weibull shape parameter ($a = 2$ in this study).

3.3 | Transformer

Power transformers play a crucial role in a power system. They are operated to step down/up the voltage level to a suitable level according to the end-user. Usually, the efficiency of a transformer is already high. Nevertheless, as the global trend for energy reduction and energy efficiency keeps increasing, the European Union has set a minimum requirement for transformer efficiency by defining a performance indicator for transformers called Peak Efficiency Index (PEI).

In order to simulate the transformer losses, the transformer capacity (S_r), magnetisation resistance (R_m), equivalent resistance (R_{eq}), and equivalent reactance (X_{eq}) must be known. The transformer capacity (S_r) was determined by the authors to meet the system requirements and match the sizes available

in Ref. [23]. The PEI is used to compute R_{eq} and X_{eq} at specified transformer sizes. The value of magnetisation resistance is assumed to be 1000 pu. The transformer equivalent resistance (R_{eq}) and equivalent reactance (X_{eq}) are calculated in the following steps:

1) acquire the PEI value from Ref. [23] according to the transformer power rating,
2) assign the short-circuit impedance (Z) according to the size of the transformer: for 3.151 to 6.30 MVA, Z = 0.0715 pu; for 6.301 to 12.5 MVA, Z = 0.0835 pu; for 12.5 to 25 MVA, Z = 0.10 pu; and for 25 to 250 MVA, Z = 0.125 pu [24],
3) find the no-load loss (P_0) at the rated primary voltage using Equation (8),
4) find the copper loss (P_k) at the rated current using Equation (9),
5) find the equivalent resistance (R_{eq}) from the copper loss using Equation (10),
6) find the equivalent reactance (X_{eq}) using Equation (11).

The equivalent resistance and reactance from the calculation will be filled in the transformer model in Simulink. Table 1 lists the parameters that are used in the simulation.

$$P_0 = \frac{V_{\text{rated}}^2}{R_m} \tag{8}$$

$$PEI = 1 - \frac{2 \cdot (P_0 + P_{c0} + P_{ckPEI})}{S_r \cdot \sqrt{\frac{P_0 + P_{ckPEI} + P_{c0}}{P_k}}} \tag{9}$$

$$P_k = I_{\text{rated}}^2 \cdot R_{eq} \tag{10}$$

$$X_{eq} = \sqrt{Z^2 - R_{eq}^2} \tag{11}$$

where PEI is the PEI (pu), P_0 is the no-load loss (W) measured at the rated voltage and rated frequency, P_{c0} is the electrical power (W) required by the cooling system for no-load operation (equal to 0 in this study), P_k is the measured load loss (W) at the rated current and rated frequency, P_{ckPEI} is the additional electrical power (W) required by the cooling system for operation (equal to 0) at k_{PEI}, S_r is the rated power (MVA) of the transformer on which P_k is based, and k_{PEI} is the load factor at which PEI occurs.

There are several types of transformer losses. Nevertheless, only core loss or no-load loss (P_0) and copper loss or load loss (P_l) are considered in this paper. Thus, the total transformer loss is computed as given in Equation (12). Transformer efficiency is calculated using Equation (13) [25].

$$P_{\text{loss},tf} = P_0 + P_l \tag{12}$$

$$\eta_{tf}(k) = \frac{k \cdot S_{tf}}{k \cdot S_{tf} + k^2 \cdot P_k + P_0} \tag{13}$$

where $P_{\text{loss},tf}$ is the total transformer loss (W), P_l is the copper loss or load loss (W) and $\eta_{tf}(k)$ is the transformer efficiency (pu) at load factor k. The efficiency (η_{tf}) obtained when load loss (P_l) equals core loss (P_0) is PEI.

3.4 | PV inverter and static frequency converter

For a large-scale PV farm, the central inverter topology is commonly employed [26]. The DC power output from the PV panels is combined by string combiners. The recombiners gather the power from each string combiner to feed into the central inverter, where the DC power is converted to three-phase AC power. There is always a loss in electrical equipment, and the inverter is no exception. There are two parts of the inverter losses: the constant part (supply to the control system and the auxiliary devices) and the load-dependent part (conduction losses and switching losses from IGBT). To calculate the inverter efficiency for each input level, Equation (14) is used [27].

The main function of the SFC is to convert three-phase power from the RESs to a single-phase power supply to the 25 kV railway overhead line via switchgear at the traction substation. Due to the unavailability of SFC efficiency information,

TABLE 1 Transformer efficiency and parameters

Transformer	PEI (%)	P_0 (W)	P_k (W)	R_m (Ω)	Z (%)	R_{eq} (Ω)	X_{eq} (Ω)
2.1 MVA, 690 V/33 kV	99.319	2100	24,347	227	6.25	0.002629	0.013924
2.5 MVA, 460 V/33 kV	99.514	2500	14,762	85	6.25	0.000500	0.005266
5 MVA, 33 kV/132 kV	99.548	5000	25,538	217,800	7.15	1.112435	15.532916
10 MVA, 33 kV/132 kV	99.615	10,000	37,056	108,900	8.35	0.403543	9.084191
15 MVA, 33 kV/132 kV	99.656	15,000	44,376	72,600	10.00	0.214780	7.256822
20 MVA, 33 kV/132 kV	99.684	20,000	49,928	54,450	10.00	0.135929	5.443303
25 MVA, 33 kV/132 kV	99.700	25,000	56,250	43,560	10.00	0.098010	4.354897
40 MVA, 132 kV/25 kV	99.724	40,000	76,176	435,600	12.50	0.829557	54.443680
80 MVA, 400 kV/132 kV	99.758	80,000	117,128	2,000,000	15.00	2.928200	299.985709

it is assumed that the efficiency curve of the SFC has the same characteristics as that of the inverter. Thus, Equation (15), derived from Equation (14), is used to determine the SFC efficiency. Equations (16) and (17) are used to determine the inverter and SFC losses, respectively.

$$\eta_{\mathrm{Inv}}\left(P_{\mathrm{dc,pu}}\right) = A_{\mathrm{Inv}} + B_{\mathrm{Inv}} \cdot P_{\mathrm{dc,pu}} + \frac{C_{\mathrm{Inv}}}{P_{\mathrm{dc,pu}}} \tag{14}$$

$$\eta_{\mathrm{SFC}}\left(P_{3p-\mathrm{AC,pu}}\right) = A_{\mathrm{SFC}} + B_{\mathrm{SFC}} \cdot P_{3p-\mathrm{AC,pu}} + \frac{C_{\mathrm{SFC}}}{P_{3p-\mathrm{AC,pu}}} \tag{15}$$

$$P_{\mathrm{loss,Inv}} = \left(1 - \eta_{\mathrm{Inv}}\right) \cdot P_{\mathrm{dc}} \tag{16}$$

$$P_{\mathrm{loss,\ SFC}} = \left(1 - \eta_{\mathrm{SFC}}\right) \cdot P_{3p-\mathrm{AC}} \tag{17}$$

where η_{Inv} is the inverter efficiency (%), η_{SFC} is the SFC efficiency (%), P_{dc} and $P_{\mathrm{dc,pu}}$ are the DC input powers (W, pu), $P_{3p-\mathrm{AC}}$ and $P_{3p-\mathrm{AC,pu}}$ are the three-phase AC input powers of SFC (W, pu), and $P_{\mathrm{loss,\ Inv}}$ and $P_{\mathrm{loss,\ SFC}}$ are the total losses (W) in the inverter and SFC, respectively. A_{Inv}, A_{SFC}, B_{Inv}, B_{SFC}, C_{Inv}, and C_{SFC} are the parameters determined from the method in Ref. [27].

In order to find parameters A, B, and C, three pairs of η_{Inv} and P_{dc} values per unit are required. In this study, inverter efficiencies of 0.1, 0.2, and 1 pu of P_{dc} are used. They are taken from the efficiency curve of the manufacturer's datasheet [28] for a 2.2 MVA inverter with a peak efficiency of 98.6%. The same procedures are applied to determine the SFC efficiency curve. The SFC is a modular system with the assumption of 5 MVA per unit. Thus, the number of units can be customised to obtain the required power rating suitable for the installed RES. The efficiency of 98% at the rated capacity taken from the converter at an equivalent rating [29] is assigned and used in (15).

The estimation of A, B, and C for the inverter and the SFC is implemented using the Curve fitting tool in MATLAB. A_{Inv}, A_{SFC}, B_{Inv}, B_{SFC}, C_{Inv}, and C_{SFC} are 98.86, 98.82, −0.8611, −0.7222, −0.09722, and −0.09444, respectively. The efficiency curves of the 2.2 MVA PV inverter, 5 MVA SFC, and power transformers are shown in Figure 4.

3.5 | Transmission line

Another critical component is the transmission line. The L12 pylon, used in the United Kingdom for 275 kV and 400 kV transmission systems, is used in this study to find the electrical parameters [30]. To calculate the per-phase capacitance, inductance and resistance per unit length, the All-Aluminium Alloy Conductor with 700 mm^2 nominal area and 37.26 mm diameter with the code name 'Araucaria' is adopted on the pylon to carry the current from the power station to the GSP [31]. The DC resistance of this conductor is 0.04,047 Ω/km [32]. The capacitance and inductance from the calculation using the

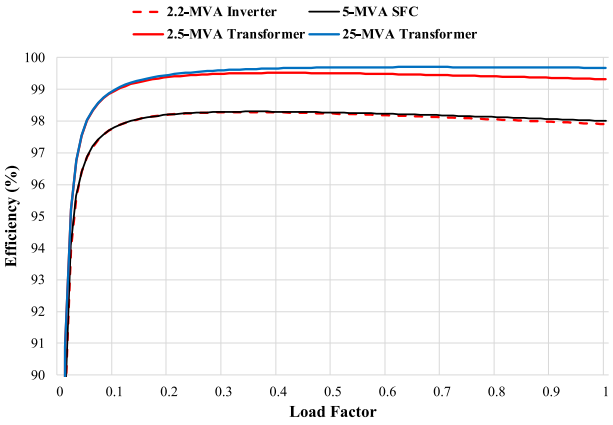

FIGURE 4 The efficiency of the inverter, static frequency converter (SFC), and transformers used in this study versus load factor

equations from Ref. [25] are 0.024 μF per phase per km and 0.466 mH per phase per km, respectively. Equation (18) shows the losses in transmission line calculation.

$$P_{\mathrm{loss,\ TL}} = \left|I_{\mathrm{cond}}\right|^2 \cdot R_{\mathrm{cond}} \tag{18}$$

where I_{cond} is the current flow in the conductor (A), R_{cond} is the conductor resistance (Ω), and $P_{\mathrm{loss,TL}}$ is the transmission line losses (W).

3.6 | Voltage unbalance factor (VUF)

Due to a single-phase traction load, load imbalance occurs, and it causes negative-phase sequence currents and voltages in the upstream power system. Rotating machines are susceptible to these negative-phase sequence components and may malfunction. The VUF, commonly used to measure the imbalance of a power system, is the ratio of negative-phase sequence voltage to positive-phase sequence voltage [33], as seen in (19).

$$\mathrm{VUF}\ (\%) = \frac{\left|V_{\mathrm{Neg}}\right|}{\left|V_{\mathrm{Pos}}\right|} \times 100 \tag{19}$$

where V_{Neg} is the negative-phase sequence voltage (V) and V_{Pos} is the positive-phase sequence voltage (V).

According to the UK grid code [34], the VUF for England and Wales transmission systems should not exceed 1.5% for voltage levels above 150 kV and 2% for 132 kV.

3.7 | Cost evaluation

The cost of renewable energy generation plants is comprised of several components. In this study, six main elements of cost are considered to estimate the lifetime cost of solar PV and wind farms. The first one is the predevelopment costs, which are the cost of licencing and technical design. The second one is the construction costs, which include the infrastructure cost, grid connection cost, transformer cost, substation cost,

inverter cost, and balance of system cost. The operation and maintenance (O&M) costs, consisting of fixed O&M and variable O&M, are considered as the third and fourth components, respectively. The amount of energy generated (MWh) determines the variable O&M costs [35]. Additionally, the insurance cost is included to cover the risk of unforeseen events. Lastly, the cost of using the transmission network is considered as the Network Use of System charges [36]. Equations (20) and (21) are used to calculate the lifetime costs of PV and wind farms. Their abbreviations and values are shown in Table 2.

$$\begin{aligned} C_{\mathrm{LF,PV}} = {} & c_{\mathrm{PD,PV}} \cdot P_{\mathrm{PV,rated}} + c_{\mathrm{CN,PV}} \cdot P_{\mathrm{PV,rated}} \\ & + c_{\mathrm{IN,PV}} \cdot P_{\mathrm{PV,rated}} + c_{\mathrm{UoS,PV}} \cdot P_{\mathrm{PV,rated}} \\ & + c_{\mathrm{OMfix,PV}} \cdot P_{\mathrm{PV,rated}} \cdot T_{\mathrm{LF,\ PV}} + c_{\mathrm{OMvar,PV}} \cdot E_{\mathrm{PV,LT}} \end{aligned} \tag{20}$$

$$\begin{aligned} C_{\mathrm{LF,Wind}} = {} & c_{\mathrm{PD,Wind}} \cdot P_{\mathrm{Wind,rated}} + c_{\mathrm{CN,Wind}} \cdot P_{\mathrm{Wind,rated}} \\ & + c_{\mathrm{IN,Wind}} \cdot P_{\mathrm{Wind,rated}} + c_{\mathrm{UoS,Wind}} \cdot P_{\mathrm{Wind,rated}} \\ & + c_{\mathrm{OMfix,Wind}} \cdot P_{\mathrm{Wind,rated}} \cdot T_{\mathrm{LF,\ Wind}} \\ & + c_{\mathrm{OMvar,Wind}} \cdot E_{\mathrm{Wind,LT}} \end{aligned} \tag{21}$$

The lifetime costs of the V/V transformer, SFC, and 33 kV/132 kV transformer are calculated using (22), (23), and (24), respectively. These costs are composed of two parts: the capital cost and O&M cost. The O&M costs for the three pieces of equipment are assumed to be 10% of the capital cost.

$$C_{\mathrm{VV,TF}} = C_{\mathrm{Cap,\ VV}} + C_{\mathrm{OM,VV}} \tag{22}$$

$$C_{\mathrm{SFC}} = C_{\mathrm{cap,SFC}} + C_{\mathrm{OM,SFC}} \tag{23}$$

$$C_{\mathrm{TF}} = C_{\mathrm{cap,TF}} + C_{\mathrm{OM,TF}} \tag{24}$$

where $C_{\mathrm{VV,TF}}$, $C_{\mathrm{cap,VV}}$, and $C_{\mathrm{OM,VV}}$ are the lifetime cost, capital cost, and O&M cost of the V/V transformer in scheme-2; C_{SFC}, $C_{\mathrm{cap,SFC}}$, and $C_{\mathrm{OM,SFC}}$ are the lifetime cost, capital cost, and O&M cost of the SFC in scheme-3; and C_{TF}, $C_{\mathrm{cap,TF}}$, and $C_{\mathrm{OM,TF}}$ are the lifetime cost, capital cost, and O&M cost of the power transformer (33 kV/132 kV) in scheme-1.

Equation (25) shows the lifetime cost of scheme-1. Due to the extra transformer (V/V transformer) in scheme-2, the lifetime cost of the V/V transformer is added to Equation (25) and becomes Equation (26). To compute the cost of scheme-3, the 33 kV/132 kV power transformer lifetime cost is subtracted from that of scheme-1 and the lifetime cost of SFC is added instead as presented in Equation (27). It should be noted that Equations (25) to (27) show the lifetime cost for one traction substation only.

$$C_{\mathrm{RES,\ S1}} = C_{\mathrm{LF,PV}} + C_{\mathrm{LF,Wind}} \tag{25}$$

$$C_{\mathrm{RES,S2}} = C_{\mathrm{LF,PV}} + C_{\mathrm{LF,Wind}} + C_{\mathrm{VV,TF}} \tag{26}$$

$$C_{\mathrm{RES,S3}} = C_{\mathrm{LF,PV}} + C_{\mathrm{LF,Wind}} + 2 \cdot C_{\mathrm{SFC}} - 2 \cdot C_{\mathrm{TF}} \tag{27}$$

where $C_{\mathrm{RES,S1}}$, $C_{\mathrm{RES,S2}}$, and $C_{\mathrm{RES,S3}}$ are the lifetime cost of RESs in scheme-1, scheme-2, and scheme-3, respectively.

Table 3 summarises the SFC and transformer costs used in this paper. The capital cost of transformers and SFCs is modified from Ref. [37], where SFCs are assumed to cost 1.5 times that of the converter due to the unavailability of SFC data.

The railway system operator normally buys electricity from the national grid. Equation (28) shows the amount that needs to be paid by the railway system operator. This study also considers the carbon cost or carbon tax as seen in the second term. Furthermore, it is assumed that the regenerative braking energy that has not been utilised is fed back to the grid, and the railway gets paid for this depending on the amount of energy (E_{sell}). In the case of the integrated RES, the excess energy is also sold to the grid at the same price as the regenerative energy.

$$C_{\mathrm{Electricity}} = c_{\mathrm{buy}} \cdot E_{\mathrm{buy}} + c_{\mathrm{cbn}} \cdot M_{\mathrm{cbn}} - c_{\mathrm{sell}} \cdot E_{\mathrm{sell}} \tag{28}$$

TABLE 2 Abbreviation list for Equations (20) and (21)

Parameter	Units	Definition
$C_{\mathrm{LF,PV}} C_{\mathrm{LF,Wind}}$	£	Lifetime costs of PV and wind farms
$c_{\mathrm{PD,PV}} c_{\mathrm{PD,Wind}}$	£50/kW £120/kW	Predevelopment costs of PV and wind farms [35]
$c_{\mathrm{CN,PV}} c_{\mathrm{CN,Wind}}$	£400/kW £1000/kW	Construction costs of PV and wind farms
$c_{\mathrm{OMfix,PV}} c_{\mathrm{OMfix,Wind}}$	£6700/MW/year £23500/MW/year	Fixed operation and maintenance cost for PV and wind farms
$c_{\mathrm{OMvar,PV}} c_{\mathrm{OMvar,Wind}}$	£0/MWh £6/MWh	Variable operation and maintenance cost for PV and wind farms
$c_{\mathrm{IN,PV}} c_{\mathrm{IN,Wind}}$	£1824/MW £1376/MW	Insurance cost for PV and wind farms
$c_{\mathrm{UoS,PV}} c_{\mathrm{UoS,Wind}}$	£1513/MW £3109/MW	Use of system charges (transmission system) for PV and wind farms [36]
$P_{\mathrm{PV,\ rated}} P_{\mathrm{Wind,\ rated}}$	MW	Power rating of PV and wind farms
$E_{\mathrm{PV,LT}} E_{\mathrm{Wind,LT}}$	MWh	Amount of electricity generated from PV and wind farms during their lifetime
$T_{\mathrm{LF,PV}} T_{\mathrm{LF,Wind}}$	Years	Lifetime of PV and wind farms

TABLE 3 Transformers and static converter cost

33 kV/132 kV transformer		V/V transformer		Static converter (SFC)	
Size (MVA)	Cost (£m)	Size (MVA)	Cost (£m)	Size (MVA)	Cost (£m)
5	0.08	10	0.15	5	0.86
10	0.15	20	0.3	10	1.73
15	0.23	30	0.45	15	2.59
20	0.31	40	0.6	20	3.45
25	0.39	50	0.75	25	4.31

where $C_{\text{Electricity}}$ is the net cost of electricity (including carbon cost) that the railway system operator needs to pay in one year, c_{buy} is the electricity price (£140/MWh [38]), c_{cbn} is the carbon tax (£18/ton CO_2 [35]), c_{sell} is the price of energy sold to the grid (£70/MWh), E_{buy} is the amount of energy purchased (MWh), E_{sell} is the amount of energy sold to the grid (MWh), and M_{cbn} is the amount of carbon emissions for generating electricity to supply the railway.

4 | CASE STUDY

In order to compare the energy flow of each renewable energy integration scheme, a part of the UK High-Speed Two project from London to Birmingham, which is in the development phase [39], is used as a benchmark scheme in this case study. This route is around 176 km [40] with 4 stations: London Euston, Old Oak Common, Birmingham International and Birmingham Curzon Street. Three 400/132 kV GSP substations are located at Ickenham, Quainton and Burton Green, as seen in Figure 5a.

4.1 | A. simulation description

The energy profile of multiple train servicing for an entire day is created using MATLAB with the train timetable in Table 4. It can be observed in Figure 5a that each traction substation supplies power to two feeding sections at its left and right. Thus, there is a total of six feeding sections for this system. Each feeding section is separated by a neutral section (NS). In this paper, the location of the NS is known from the HS2 project data [40]. Figure 5b illustrates the power profile and speed profile with the train elapsed time of a train journey from London Euston to the destination at Birmingham Curzon Street. The power profile is sampled at 20-s intervals to ensure that it will not miss the regenerative braking data. The train starts to travel from the first station and stops at Old Oak Common after 4 min (9.5 km). Then, 12 min after departing, the train passes the first traction substation (27 km see Figure 5a). During the first 12 min, the train is supplied power by the feeding section 1. Therefore, the train will eventually be supplied by all six feeding sections during one trip. As the relationship between train elapsed time and position is perceived, multi-train services for the entire day can be implemented based on the assumption that the driving style of each train is the same. This is to ensure

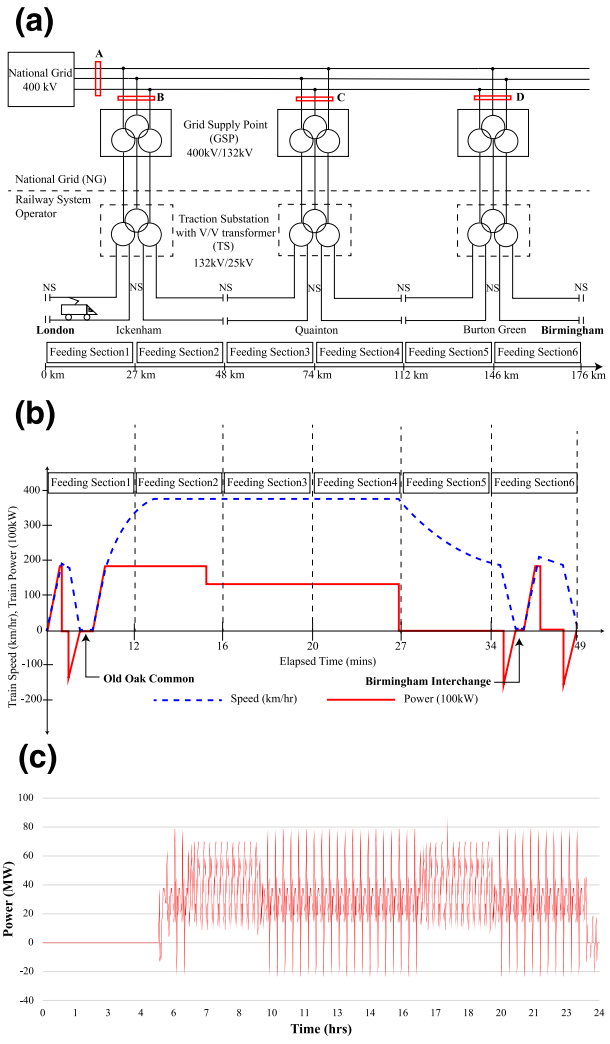

FIGURE 5 (a) Conventional connection scheme (benchmark), showing the entire power system connection of the case study, (b) train energy profile of a single train trip from London Euston to Birmingham Curzon Street from the Single Train Simulator, (c) train power demand for 24-h operation

that the relation between the elapsed time and position can be applied to all trains.

The total power demand of multiple trains operated for 24 h is shown in Figure 5c. This power demand is the result of combining the power demand of multiple trains together according to the timetable and headway in Table 4. As can be seen in Figure 5c, the first train departs at 5 a.m. and the next

trains depart 20 min later than the train before. However, during peak time, the headway is reduced to 15 min. This can be noticed from 6 to 9 a.m. and 4–7 p.m. Moreover, the regenerative braking energy is utilised by trains in the same feeding section during peak time. Overall, there are 61 train trips in each direction or 122 trips for both directions. The impedance of the feeding line (contact wire and messenger wire) is given as 0.15 + j0.45 Ω/km to simulate the losses during current flows in the contact wire. Table 5 displays the train station locations and maximum speed.

The capacity of the PV and wind farm at each traction substation for scheme-1 and scheme-2 is varied, at 4, 8, 12, 16, and 20 MW. Thus, the total installed capacity of the RES for each traction substation is 8, 16, 24, 32, and 40 MW. For scheme-3, each side of the feeding section is connected with a PV farm and wind farm, each rated at 2, 4, 6, 8, and 10 MW. The total capacity per traction substation is identical to that of scheme-1 and scheme-2.

The solar irradiance and wind speed data for each day from 2015 to 2019 were acquired from Refs. [42, 43]. Owing to the huge amount of data, the simulation would take a tremendous amount of time; thus, they are averaged and represented by months. For example, the solar irradiance and wind speed of every day in a month are averaged and represented for that month. Furthermore, since the data available are sampled at a one-hour interval, they are interpolated into 20-s intervals to match the train energy profile. The simulation of each scheme is carried out for 60 months in 5 years.

Additionally, as it is assumed that PV farms and wind farms are situated close to the traction substations, the solar irradiance and wind speed data are taken from the location of each traction substation or GSP (both are very close to each other).

4.2 | Power losses

The simulations were run on MATLAB Simulink with 20-s intervals starting from the 0^{th} to the $86{,}400^{th}$ seconds, which is the time from 00:00–24:00 h. Since this paper focuses on the losses of the steady-state model of each scheme, the results are separated into three parts: 1) the conversion losses (transformer loss and inverter loss including SFC), 2) the transmission losses, and 3) the total losses. However, only the losses in 2019 are shown due to limited space.

The bar chart in Figure 6a shows the conversion losses, which combine energy losses in transformers and inverters (also in the SFC), using the average meteorological data between January 2019 and December 2019 from Refs. [42, 43]. Overall, scheme-2 gives the highest conversion losses, except in March and August, in which it is surpassed by scheme-3. The lowest conversion losses for the proposed RES integration scheme happen with scheme-1. The conventional scheme (without RES) has the least loss among all schemes because it does not need additional equipment to accommodate the RESs. Furthermore, it is noticeable that the conversion losses of scheme-3 follow the trend of the percentage of renewable energy penetration, shown as the black dashed line. This can be explained in Figure 6b. When the amount of renewable energy rises, the power loss in the inverter and the SFC also increases. The inverter loss in scheme-3 is significantly higher than in the other schemes, and it determines the trend of the conversion loss. By observing all the simulation results for every single month from 2015 to 2019, it is found that when the RES energy penetration exceeds 90%, scheme-3 produces the largest conversion losses, as seen in March and August in Figure 6a. Considering the transformer loss, Figure 6c illustrates that scheme-2 generates the biggest transformer losses due to having

TABLE 4 HS2 train service timetable [41]

First train departs	05:00
Last train departs	23:00
Peak time	06:00–09:00 and 16:00–19:00
Headway for off-peak time	20 min
Headway for peak time	15 min

TABLE 5 Train station and maximum speed information [40]

Stations	Location (km)	Max speed (km/h)
Euston	0	230
Old Oak common	9.5	360
Birmingham interchange	156.7	230
Birmingham Curzon street	176	0

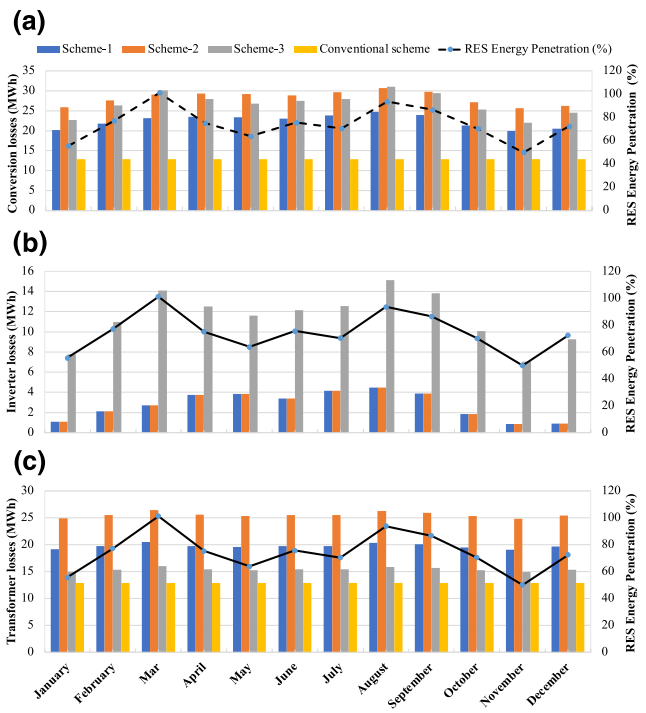

FIGURE 6 Conversion losses for different schemes and the renewable energy penetration percentage using meteorological data for the year 2019: (a) conversion losses, (b) inverter losses (including the Static Frequency Converter (SFC) losses for scheme-3), and (c) transformer losses

an extra transformer (V/V transformer), followed by scheme-1, scheme-3, and lastly the conventional scheme.

In contrast to the conversion losses, as the grid is the only supply, the conventional scheme generates the maximum transmission losses as presented in Figure 7a. In this case, the energy source is far from the load centre. As a result, the current flows through the long-distance conductor to the load and a small part of the energy is dissipated as heat. In comparison, the difference in transmission losses is marginal for each scheme since the resistance of the conductor is very small. To see the losses in the conductor more clearly, Figure 7b shows the transmission losses that occur during the flow of electricity from the grid to the load and vice versa. It can be seen that the loss is similar though the amount of RES is different. In addition, it is obviously seen that the transmission loss caused by the excess renewable energy flowing to the grid has the same trend as the percentage of renewable energy penetration. Because the transmission losses for all schemes are marginally different, the total losses follow the trend of the conversion losses, as shown in Figure 8.

4.3 | Voltage unbalance factor

The VUF is determined at four locations, from A to D (see Figure 5a); the results are tabulated in Table 6. At the 400 kV level, which is used as the transmission system for this study, the VUFs for all locations and all schemes are below the defined limit at 1.5%.

The results are identical or slightly different at the same measured locations. This indicates that the integration of the RES has not worsened the system imbalance. The reason is that the 400 kV transmission system has a significantly high short-circuit capacity. The design limit of the fault level for a 400 kV system in the United Kingdom is 34,500 MVA or 50 kA [44]. Consequently, the effect of imbalance caused by the railway load and the connection of the RES is insignificant. In addition, 132 and 275 kV voltage levels are also commonly employed in the United Kingdom. Thus, the VUF of these voltage levels is calculated as well. For the 275 kV system, the VUF for most locations stays below the limit, except for location D, in which the VUFs marginally exceed 1.5%. On the other hand, all the VUFs for the 132 kV system are beyond the maximum permissible level of 2%. Hence, without a compensation device, such as a load balancer, a railway power system with a high traction load should not be connected to the 132 and 275 kV transmission systems. It is worth mentioning that the Static Var Compensator, Static Synchronous Compensator and Railway Power Conditioner can be utilised as load balancers [45].

From the VUF results in Table 6, if the 132 kV transmission system supplies the traction loads, the load balancers will be required for all three traction substations to suppress the unbalance so that the VUFs at spots A, B, C and D are reduced below the tolerance. On the other hand, only one traction substation at Burton Green will require a load balancer to deduct the VUF at spot D if the traction loads are connected to a 275 kV transmission system. Nevertheless, a feasibility study and cost assessment must be done to choose which transmission level the traction substations will be connected to. For instance, the lifetime cost of using 400 kV may be less than that of 132 and 275 kV with load balancers due to maintenance costs.

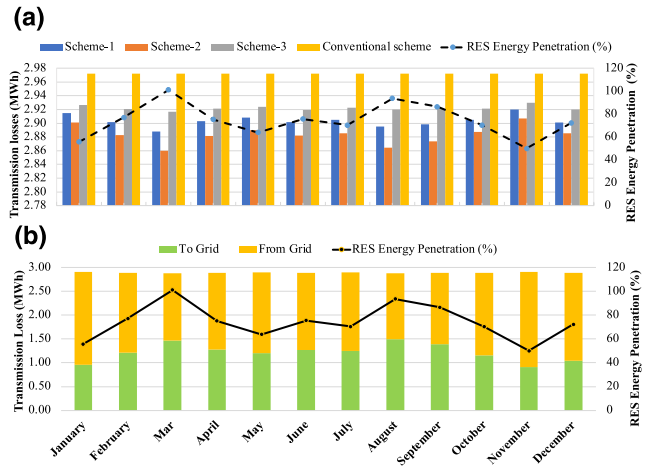

FIGURE 7 (a) Transmission losses and (b) transmission losses from scheme-1 (2019) due to the flow of electricity to and from the grid to supply the railway load, using meteorological data from 2019

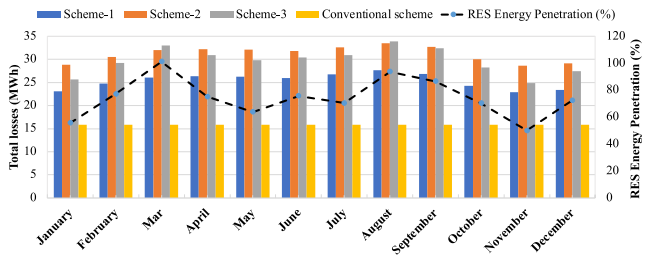

FIGURE 8 Total losses (combination of conversion losses in Figure 6a and transmission losses in Figure 7a)

4.4 | Cost evaluation

In order to compare the lifetime cost of the system, the project lifetime of the PV and wind farms is assumed to be 25 years, from 2026 to 2050. According to Ref. [38], the average electricity price of £140 per MWh is applied for the United Kingdom. It is assumed by the authors that the electricity can be sold to the grid for half the buying price. Moreover, since the United Kingdom has a target to reduce carbon emissions, the amount of equivalent carbon is calculated, and the carbon tax is applied. The forecast carbon intensity data [46] illustrated in Figure 9 are used to compute the amount of carbon emitted from the power generation.

The cost calculation results are illustrated in Figure 10 for different sizes of RES (PV farm and wind farm), varying from 24 to 120 MW for the whole project. It should be noted that the RES installed capacity shown is for the entire project (three locations of RES). The first 3 bars (blue, orange, and grey) show

TABLE 6 Voltage unbalance factor (VUF) results

Transmission voltage	Scheme	Voltage unbalance factor (VUF, %)			
		Location A	Location B	Location C	Location D
132 kV	Benchmark	2.75	2.93	4.24	7.12
	Scheme-1	2.74	2.92	4.22	7.07
	Scheme-2	2.74	2.92	4.19	7.00
	Scheme-3	2.71	2.88	4.06	6.83
275 kV	Benchmark	0.72	0.76	1.00	1.58
	Scheme-1	0.72	0.76	1.00	1.58
	Scheme-2	0.72	0.76	0.90	1.57
	Scheme-3	0.72	0.76	1.01	1.54
400 kV	Benchmark	0.32	0.34	0.46	0.73
	Scheme-1	0.32	0.34	0.46	0.73
	Scheme-2	0.32	0.34	0.45	0.73
	Scheme-3	0.32	0.34	0.46	0.71

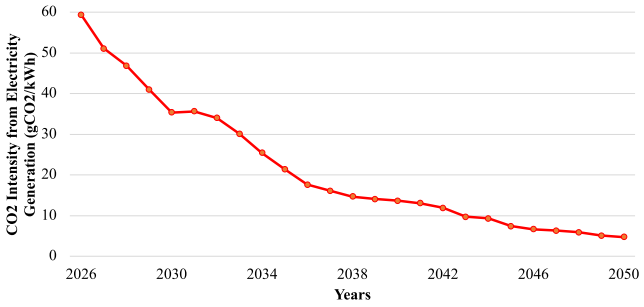

FIGURE 9 Estimated carbon intensity from the power generation sector in the United Kingdom [46]

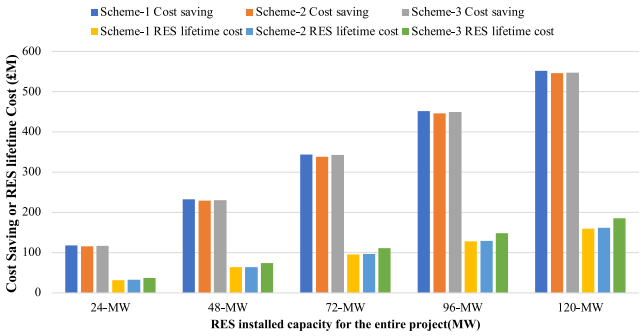

FIGURE 10 Total cost saving compared to the conventional scheme, and lifetime cost of renewable energy source (RES) for each proposed scheme

the electricity cost saving for each proposed scheme compared to the conventional scheme. In other words, it is the total electricity cost of the conventional scheme minus the total electricity cost of the RES integration schemes in 25 years of operation, the cost saving increases with the size of the RES installed. For the RES with installed capacity of 24 MW, the energy cost is around £115 m lower than that of the

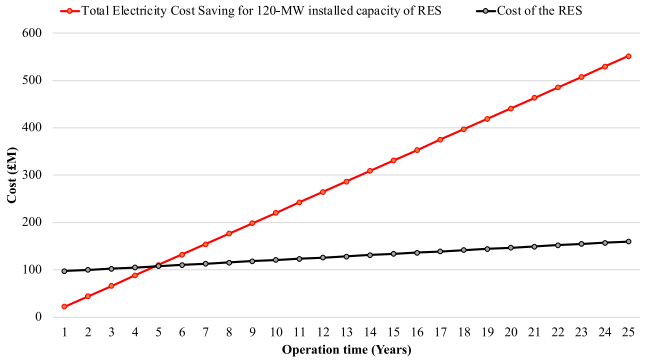

FIGURE 11 Total electricity cost saving of scheme-1 and cost of 120 MW renewable energy source (RES) (60 MW PV farm and 60 MW Wind farm) over time

conventional scheme during the 25-year project and about £550 m lower for the 120 MW RES. The lifetime cost of the RES is shown in the last 3 bars (yellow, light blue, and green) for each RES installed capacity. This cost is calculated using Equations (24), (25), and (26) in Section 3. It can be seen that the lifetime cost of scheme-1 is the lowest for all RES installed capacities, followed by that of scheme-2, and lastly scheme-3. Due to the extra transformer required, scheme-2 costs more than scheme-1. With the SFC in scheme-3, this scheme has the highest lifetime cost as the SFC cost is exceptionally high. Overall, the electricity cost saving is much higher than the RES lifetime cost for all proposed schemes and installed capacities. This indicates that it is worth the railway system operator investing in integrating the RESs into the railway power system.

Figure 11 depicts the payback time for the 120 MW RES in scheme-1 when the cost of the PV farm and wind farm (including the O&M cost) is matched by the electricity cost saving. The RES cost is paid off at around 5 years as seen at the breakeven point.

TABLE 7 Amount of energy and carbon for 25 Years

Type	RES size	Transaction	Scheme-1	Scheme-2	Scheme-3	Benchmark
Energy (GWh)	24 MW	Buy from grid	5285.6	5295.4	5291.5	6062.2
		Sell to grid	187.0	183.5	186.4	63.8
	48 MW	Buy from grid	4546.4	4565.6	4559.4	6062.2
		Sell to grid	348.8	341.6	346.8	63.8
	72 MW	Buy from grid	3845.9	3882.5	3855.8	6062.2
		Sell to grid	537.0	520.7	535.5	63.8
	96 MW	Buy from grid	3215.6	3248.6	3232.4	6062.2
		Sell to grid	814.1	794.0	804.3	63.8
	120 MW	Buy from grid	2701.3	2730.2	2721.2	6062.2
		Sell to grid	1206.8	1182.1	1185.1	63.8
Carbon	24 MW	Amount (1000 t)	113.92	114.77	113.64	130.20
		Tax (Million-£)	2.05	2.07	2.05	2.34
	48 MW	Amount (1000 t)	97.93	98.76	97.92	130.20
		Tax (£m)	1.76	1.78	1.76	2.34
	72 MW	Amount (1000 t)	82.59	83.38	82.81	130.20
		Tax (£m)	1.49	1.50	1.49	2.34
	96 MW	Amount (1000 t)	69.06	69.77	69.42	130.20
		Tax (£m)	1.24	1.26	1.25	2.34
	120 MW	Amount (1000 t)	58.00	58.60	58.40	130.20
		Tax (£m)	1.04	1.05	1.05	2.34

Table 7 displays the amount of energy flow of each scheme with various RES sizes and the amount of carbon emissions and costs for 25 years. The amount of carbon emissions can be reduced by half, from 130,200 tonnes with the benchmark scheme to 58,400 tonnes for the schemes with RES.

5 | CONCLUSIONS

Renewable energy integration schemes for the AC high-speed rail were proposed, and simulations were implemented to obtain the system's energy flow and power losses. The results show that among the RES integration schemes, scheme-1, in which the PV and wind farms are connected to a three-phase railway power network, provides the smallest total losses. Moreover, it also has the lowest lifetime cost for a 25-year lifetime. The scheme with RES connected to the railway side via a V/V transformer is the worst in terms of total losses as greater losses are produced in the V/V transformer, and this scheme will cost more than scheme-1. The total loss for the scheme with an SFC is slightly lower than that of scheme-2 if the RES energy penetration is less than 90%.

Considering the electricity cost-saving, the lifetime cost of each proposed scheme will be paid off in around 5 years, and an enormous electricity charge is saved in 25 years. Besides that, the VUF demonstrates that the integration of the RESs does not affect the system imbalance, and the VUF stays within the acceptable limit for the 400 kV transmission system. Nevertheless, a vast land area is required for PV and wind farms with a large generation capacity, such as in scheme-1 and scheme-2, which may be unavailable. The problem can be solved by implementing scheme-3 because the RES size on each side of the feeding sections is halved compared to the first two schemes. Furthermore, it is the most flexible scheme in terms of connection points as the RES can be connected to the railway overhead line along the route.

Due to the fluctuation of traction load, the VUF, when connecting the traction load to the grid with low short-circuit capacity, exceeds the permissible value. Even though the ESS cannot completely reduce the VUF to below the limit, it can still support the short-term power stabilisation by capturing the regenerative braking energy and discharging it to the up-coming trains. This will decrease the power difference between peak and minimum power. Hence, the power profile is less fluctuating.

The utilisation of ESS and its effects on reducing the electricity cost and transmission line losses will be explored in future work. Furthermore, the optimal sizing of the solar PV farm and wind farms' optimal sizing will also be included.

ACKNOWLEDGEMENT

This research is supported by the Decarbonising Transport through Electrification (DTE) Network+ funded by EPSRC (grant reference EP/S032053/1).

CONFLICT OF INTEREST

The author declares that there is no conflict of interest that could be perceived as prejudicing the impartiality of the research reported.

DATA AVAILABILITY STATEMENT

Research data are not shared.

PERMISSION TO REPRODUCE MATERIALS FROM OTHER SOURCES

None.

ORCID

Zhongbei Tian https://orcid.org/0000-0001-7295-3327

REFERENCES

1. Committee on Climate Change: Net Zero: The UK's Contribution to Stopping Global Warming, pp. 11 (2019)
2. International Energy Agency: Renewables 2020: Analysis and Forecast to 2025, pp. 11–12 (2020)
3. Department for Business: Energy & Industrial Strategy. UK Energy in Brief (2021)
4. Office of Rail and Road. Rail Emissions (2019)
5. D'Arco, S., Piegari, L., Tricoli, P.: Comparative analysis of topologies to integrate photovoltaic sources in the feeder stations of AC railways. IEEE Trans. Transp. Electrif. 4(4), 951–960 (2018). https://doi.org/10.1109/tte.2018.2867279
6. Aguado, J.A., Racero, A.J.S., De La Torre, S.: Optimal operation of electric railways with renewable energy and electric storage systems. IEEE Trans. Smart Grid 9(2), 993–1001 (2018). https://doi.org/10.1109/tsg.2016.2574200
7. Şengör, I., et al.: Energy management of a smart railway station considering regenerative braking and stochastic behaviour of ESS and PV generation. IEEE Trans. Sustain. Energy 9(3), 1041–1050 (2018). https://doi.org/10.1109/tste.2017.2759105
8. Liu, Y., et al.: Robust energy management of high-speed railway co-phase traction substation with uncertain PV generation and traction load. IEEE Trans. Intell. Transport. Syst., 1–13 (2021)
9. Chen, M., et al.: Multi time-scale optimal dispatch of railway FTPSS based on model predictive control. IEEE Trans. Transp. Electrif. 6(2), 808–820 (2020). https://doi.org/10.1109/tte.2020.2992693
10. HS2: Grid Supply Point Connection at Parkgate (2020)
11. SMA Technology: Sunny Central 2200/2475/2500-EV/2750-EV/3000-EV, pp. 3 (2021)
12. VESTAS: General Specification: V90-1.8/2.0 MW 50 Hz VCS, pp. 16 (2010)
13. Kiessling, F., et al.: Contact Lines for Electric Railways, pp. 51–54 (2018)
14. ABB, "More Power for Railway Lines: Dynamic Shunt Compensation and Static Frequency Conversion for 50 Hertz (Hz) Traction Power Supply" (2016)
15. ABB: ABB to Provide Innovative Traction Power Solution for UK Railway Network (2017)
16. Railway Industry Association: RIA Electrification Cost Challenge, pp. 41 (2019)
17. Tian, Z., et al.: System energy optimisation strategies for metros with regeneration. Transport. Res. C Emerg. Technol. 75, 120–135 (2017). https://doi.org/10.1016/j.trc.2016.12.004
18. 24-hour Simulation of a Vehicle-To-Grid (V2G) System: https://uk.mathworks.com/help/physmod/sps/ug/24-hour-simulation-of-a-vehicle-to-grid-v2g-system.html, Accessed 4 July 2021
19. Department for Business, Energy & Industrial Strategy: Wind Powered Electricity in the UK (2020). https://assets.publishing.service.gov.uk/government/uploads/system/uploads/attachment_data/file/875384/Wind_powered_electricity_in_the_UK.pdf
20. Gharehpetian, G.B., Mousavi, S.M.: Distributed Generation Systems, pp. 31. Butterworth-HeinemannOxford (2017)
21. Schaffarczyk, A.: Understanding Wind Power Technology, 1st ed, pp. 76. Wiley (2014)
22. Johnson, G.L., Ma, K.: Wind energy systems. Proc. IEEE 105(11), 2116–2131 (2017). https://doi.org/10.1109/jproc.2017.2695485
23. IEC, IEC 60076-20 TS: Power Transformers – Part 20: Energy Efficiency, (2016)
24. Bayliss, C.R., Hardy, B.J.: Power transformers. In: Transmission and Distribution Electrical Engineering, 3rd ed, pp. 499–564. Newnes (2007)
25. Hadi, S.: Power System Analysis, 1st ed, pp. 70–135. McGraw-Hill, New York (1999)
26. Yang, Y., et al.: Power electronic technologies for PV systems. In: Advances in Grid-Connected Photovoltaic Power Conversion Systems, pp. 24. Elsevier Science & TechnologySan Diego (2018)
27. Demoulias, C.: A new simple analytical method for calculating the optimum inverter size in grid-connected PV plants. Elec. Power Syst. Res. 80(10), 1197–1204 (2010). https://doi.org/10.1016/j.epsr.2010.04.005
28. SMA.: Sunny Tripower 15000TL/20000TL/25000TL, vol. 2021, pp. 3
29. ABB: ABB Wind Turbine Converters PCS6000, Full Power Converter, up to 12 MW, pp. 11 (2019)
30. Geometries of Power Line: https://www.emfs.info/sources/overhea%20d/ohl-calculating/geometries/, Accessed 12 August 2021
31. El Gayar, A., Abdul-Malek, Z., Elshami, I.: Wind-induced clearances infringement of overhead power lines. Int. J. Comput. Electron. Eng. 6(4), 275–282 (2014). https://doi.org/10.7763/ijcee.2014.v6.838
32. Clydesdale, ABC, Copper, AAAC & ACSR Conductor Specifications, pp. 2, (2021)
33. Ghassemi, F., Perry, M.: Review of Voltage Unbalance Limit in the GB Grid Code CC.6.1.5 (B), pp. 2. National Grid (2014)
34. National grid electricity transmission plc: The grid code, Issue 5
35. Department for Business: Energy & Industrial Strategy, Electricity Generation Costs 2020, pp. 10 (2020)
36. Department of Energy and Climate Change: Review of Renewable Electricity Generation Cost and Technical Assumptions, pp. 20–57, (2016)
37. National Grid: Electricity Ten Year Statement 2014 (Appendix E23 Unit Costs), pp. 69
38. Department for Business: Energy & Industrial Strategy, Quarterly Energy Prices: UK, pp. 8 (2021)
39. HS2: Realising the Potential", pp. 15 (2018)
40. UK Government: HS2 Phase One Plan and Profile Maps: London to the West Midlands. https://www.gov.uk/government/collections/hs2-plan-and-profile-maps-between-london-and-the-west-midlands
41. HS2: High-Speed Rail London to the West Midlands and beyond: HS2 Technical Appendix, pp. 7 (2009)
42. Pfenninger, S., Staffell, I.: Long-term patterns of European PV output using 30 years of validated hourly reanalysis and satellite data. Energy 114, 1251–1265 (2016). https://doi.org/10.1016/j.energy.2016.08.060
43. Staffell, I., Pfenninger, S.: Using bias-corrected reanalysis to simulate current and future wind power output. Energy 114, 1224–1239 (2016). at. https://doi.org/10.1016/j.energy.2016.08.068 https://www.renewables.ninja/
44. Power System Limited, SP.: Calculation of System Fault Levels, pp. 6Issue (2017)
45. Serrano-Jiménez, D., et al.: Electrical railway power supply systems: current situation and future trends. Int. J. Electr. Power Energy Syst. 92, 181–192 (2017). https://doi.org/10.1016/j.ijepes.2017.05.008
46. Grid, N.: Future Energy Scenarios 2021 Data Workbook. https://www.nationalgrideso.com/future-energy/future-energy-scenarios

How to cite this article: Kano, N., et al.: Comparison of renewable integration schemes for AC railway power supply system. IET Electr. Syst. Transp. 12(3), 209–222 (2022). https://doi.org/10.1049/els2.12048